

FUSE Observation of the Non-Radiative Collisionless Shock in the Remnant of SN1006

K. E. Korreck^{1,2}, J.C. Raymond², T.H. Zurbuchen¹, P. Ghavamian³

ABSTRACT

The appearance of the young supernova remnant SN1006 is dominated by emission from non-radiative shocks in the NE and NW regions. At X-ray energies the northeast shock exhibits predominantly nonthermal synchrotron emission, while the northwest shock exhibits a thermal spectrum. We present far ultraviolet spectra of the northeast (NE) and northwest (NW) portions of SN 1006 acquired with the Far Ultraviolet Spectroscopic Explorer (FUSE). We have detected emission lines of O VI (1032, 1038 Å) and broad Ly- β (1025 Å) in the NW filament, but detect no emission lines in the NE region down to a level of 4.7×10^{-17} erg cm⁻² s⁻¹ arcsecond⁻². We observed in the NW an O VI intensity of $2.0 \pm 0.2 \times 10^{-16}$ erg cm⁻² s⁻¹ arcsecond⁻² and measured an O VI line width of 2100 ± 200 km s⁻¹ at a position where the H α width was measured to be 2290 ± 80 km s⁻¹ (Ghavamian et al. 2002). This implies less than mass proportional heating of the ions. Using the ratio of intensities, $I(\text{NW})/I(\text{NE}) \sim n(\text{NW})/n(\text{NE})$, the density ratio of the two regions is found to be ≥ 4 , a value that is with the uncertainties of the ratio of 2.5 measured by Long et al. (2003). The derived O VI kinetic temperature is compared to previous estimates of electron, proton, and ion temperatures in the remnant to study the relative heating efficiency of various species at the shock front. The degree of postshock temperature equilibration may be crucial to particle acceleration since the temperature of each species determines the number of high speed particles available for injection into an acceleration process that could produce Galactic cosmic rays.

Subject headings: ISM:individual(SN1006)—supernova remnants—shock waves—ultraviolet:ISM

¹University of Michigan, Department Of Atmospheric, Oceanic and Space Sciences, 2455 Hayward, Ann Arbor MI 48109

²Harvard-Smithsonian Center for Astrophysics, 60 Garden Street, Cambridge, MA 02138

³Department of Physics and Astronomy, Johns Hopkins University, 3400 North Charles Street, Baltimore, MD, 21218-2686

1. Introduction

SN1006 (G327.6+14.6) is a nearby Type Ia supernova remnant at a distance of 2.1 kpc (Winkler, Gupta, Long 2003). With a mean expansion rate of 8700 km s^{-1} it is ~ 18 pc wide (Winkler, Gupta, Long 2003). The remnant has a high Galactic latitude and modest foreground reddening, $E(B-V)=0.11 \pm 0.02$ (Schweizer & Middleditch 1980). This young supernova remnant is entering the Sedov-Taylor phase of supernova remnant evolution.

SN1006 has been observed at radio (Pye et al. 1981), optical (Ghavamian et al. 2002; Kirshner, Winkler, and Chevalier 1987; Smith et al. 1991), ultraviolet (Raymond, Blair, Long 1995) and X-ray (Winkler, Gupta, Long 2003; Long et al. 2003; Bamba et al. 2003) wavelengths. Gamma ray observations (Tanimori 1998) were reported but not confirmed. Thin, pure Balmer line filaments were found in the optical. In the radio and X-ray, the remnant has a limb-brightened shell structure with cylindrical symmetry around a SE to NW axis probably aligned with the ambient galactic magnetic field (Reynolds & Gilmore 1986; Jones & Pye 1988). The NE shock front of SN1006 shows strong non-thermal X-ray and possible gamma ray emission while the NW shock shows very little non-thermal emission at radio or X-ray wavelengths.

Ly- β , He II, C IV, and O VI lines were observed from the faint optical Balmer line filament of the NW shock of the supernova remnant, by the Hopkins Ultraviolet Telescope (HUT), flown during the Astro-2 space shuttle mission. The observed FWHM of the lines were 2230, 2558, 2641 km s^{-1} , respectively (the O VI line width could not be measured). A kinetic temperature could be calculated from these line widths. The kinetic temperatures of these species are not equal, because they do not scale inversely with the square root of their atomic mass. Instead, the UV observations do suggest that $T_{\text{ion}} \sim \frac{m_{\text{ion}}}{m_{\text{p}}} T_{\text{proton}}$ indicating little to no temperature equilibration between species.

SN1006 provides an opportunity to investigate parameters of non-radiative collisionless shocks faster than 2000 km s^{-1} . Collisionless shocks appear in many astrophysical phenomena, from coronal mass ejections (CMEs) in the heliosphere to jets in Herbig-Haro objects. When a shock is non-radiative the detection of emission from the shock front is possible, as all of the optical and UV emission of a non-radiative shock comes from a narrow zone directly behind the shock front. Interactions at the collisionless shock front depend upon mechanisms such as plasma waves to transfer heat, kinetic energy and momentum, and it is not well understood how particles of different masses and charges are affected by these processes. The temperature of the species and the degree of temperature equilibration between electrons, protons and other ions is central to the interpretation of X-ray spectra, which effectively measure electron temperature. The energy distribution of a particle species is important to cosmic ray studies as only those particles at a high energy tail of a particle

distribution are available for cosmic ray acceleration.

The method of using $H\alpha$ lines to determine collisionless shock parameters was originated by Chevalier & Raymond (1978) and Chevalier, Kirshner, & Raymond (1980). The $H\alpha$ line has a two component profile. The width of the broad component of the $H\alpha$ line is related to the post-shock proton temperature as a result of charge exchange between neutrals and protons, which produces a hot neutral population behind the shock. The narrow component of the $H\alpha$ line is produced when cold ambient neutrals pass through the shock and emit line radiation before being ionized by a proton or electron. The ratio of the broad to narrow flux is sensitive to electron-ion equilibrium and the pre-shock neutral fraction. The FWHM of $H\alpha$ line was measured to be $2290 \pm 80 \text{ km s}^{-1}$, with models implying the speed of the shock is $v_{\text{shock}} = 2890 \pm 100 \text{ km s}^{-1}$ (Ghavamian et. al. 2002; hereafter GWRL02). The $H\alpha$ broad to narrow intensity ratio measured to be 0.84 implies an electron temperature much lower than the ion temperature.

This UV observation from the FUSE satellite focused on the shock front in the NW observed by HUT and GWRL02 and on a region in the NE dominated by non-thermal emission. From the spectra, a broad Lyman β line ($\lambda \sim 1025 \text{ \AA}$) and the doublet of O VI ($\lambda \sim 1032, 1038 \text{ \AA}$) were analyzed for spectral width, intensity, and flux. We use the line widths of the NW and the intensities of the O VI lines in the NE and NW shock fronts to compare the electron-ion and ion-ion temperature equilibration efficiencies as well as densities. The heating of different particle species by the shock front as well as parameters of collisionless shocks that affect particle species heating will be discussed.

2. Observations

The Far Ultraviolet Spectroscopic Explorer (FUSE) has a wavelength range of approximately 900-1180 \AA . The Large Square Aperture (LWRS), with a field-of-view of $30'' \times 30''$, with a roll angle of 167° , was chosen for this observation because models predicted that the O VI emission behind the shock would be spread over $35''$ (Raymond, Blair, Long 1995; Laming et al. 1996). The LWRS has a filled-aperture resolution of about 100 km s^{-1} . The FUSE spectrometer consists of four independent channels with two segments each. Four of these eight segments operate in the wavelength range for the O VI doublet, $\lambda = 1031.91, 1037.61 \text{ \AA}$. However, the Silicon Carbon (SiC) coated channels, because they are optimized for $\lambda \leq 1020 \text{ \AA}$, add an unacceptable amount of noise to our faint signal, so only the Lithium Fluoride (LiF) channels are used. These two segments are designated LiF1A and LiF2B. The LiF1A channel covers wavelengths 987.1 - 1082.3 \AA , while the LiF2B covers 979.2-1075.0 \AA .

Although the northwest region of the remnant has been observed before in the UV (Raymond, Blair, Long 1995), we have much better spectral resolution and a more optimal aperture size to include the entire ionization region given that it may be larger than $19''$ (Laming et al. 1996). The apertures used for past observations were HUT= $19'' \times 197''$ (Raymond, Blair, Long 1995) and CTIO RC Spectrometer= $2'' \times 51''$ (Winkler, Gupta, Long 2003) (GWRL02). We positioned the aperture center to be $5''$ - $10''$ behind the $H\alpha$ filament where the peak formation of O VI occurs. The NE position was chosen based on the edge of the X-ray filament from Long et al. (2003).

FUSE observations of the northwest region, centered at $\alpha_{2000} = 15^h 2^m 19.17^s$, $\delta_{2000} = -41^\circ 44' 50.4''$ were obtained on 23 June 2001 and 26 February 2002 with total exposure times of 35,627 s and 6,690 s. Observations of the northeast region, centered at $\alpha_{2000} = 15^h 4^m 5.0^s$, $\delta_{2000} = -41^\circ 50' 40.5''$ were obtained on 25 June 2001 and 27 February 2002 with exposure times of 42,365 s and 9,666 s. The locations of observations are shown superimposed on an $H\alpha$ image of the remnant taken with the CTIO Schmidt telescope in Figure 1 (Winkler, Gupta, Long 2003). Inserted in the figure is a close up from Chandra (Long et al. 2003) of the NE region of observation to illustrate the x-ray morphology, although no optical emission is obviously present.

There are four components to the background of this observation; detector background, geocoronal lines, the diffuse galactic UV continuum and diffuse galactic O VI emission. The background count distribution on the FUSE detectors is composed of two separate components (Anderson, Sankrit, Dupuis 2003). The ‘intrinsic’ background forms from the β -decay of potassium in the microchannel plate (MCP) detector glass and the spacecraft radiation environment. The effect of the spacecraft radiation environment on the detector background varies from night to day and with solar activity, but over a short observing time this variation is not significant. The second component is caused by scattered light, primarily geocoronal Ly- α . This line produces detector averaged count rates as small as 20% of the intrinsic background during the night and increasing to 1-3 times the intrinsic rate during the day. The other two components of the background, galactic UV emission and diffuse O VI emission, will be discussed later.

The observations were calibrated with the CalFUSE Pipeline Version 2.2.1. Data from all exposures are processed through the pipeline and then co-added following the FUSE Data Analysis Cookbook and The FUSE Observer’s Guide. The data were selected to contain only the night observations. This greatly reduces the geocoronal background. The night-only exposure times were 32,287 s for the Northwest and 39,386 s for the Northeast.

3. Analysis and Results

As mentioned above, the background consists of detector noise, geocoronal lines, diffuse galactic O VI and an astrophysical UV continuum. The first two sources were explained in the previous section, but the additional diffuse UV continuum must be treated separately. It does not originate from SN1006, as it is seen in both of the entirely different regions of the remnant; the NE shock and the NW shock. The diffuse background is attributed to light from hot stars scattering on dust. The diffuse UV continuum is especially bright in this region of the sky according to models by Murthy & Henry (1995). A value of 8.4×10^{-15} erg $\text{cm}^{-2} \text{s}^{-1} \text{\AA}^{-1}$ was quoted by Raymond, Blair, Long (1995) while we are seeing approximately 6.5×10^{-15} erg $\text{cm}^{-2} \text{s}^{-1} \text{\AA}^{-1}$ through an aperture one quarter the size of the HUT observation.

In addition to the diffuse UV continuum, Shelton et al. (2001, 2002) and Otte et. al. (2003) have found a diffuse O VI background. The brightness of the O VI background is 4700 ± 2400 photons $\text{cm}^{-2} \text{s}^{-1} \text{sr}^{-1}$ (Otte, Dixon, & Sankrit preprint). The widths of the diffuse O VI lines fall between 10 and 160 km s^{-1} . In the current NE spectrum diffuse O VI emission has a width of $\leq 200 \text{ km s}^{-1}$ and a brightness of 3500 photon $\text{cm}^{-2} \text{s}^{-1} \text{sr}^{-1}$. We attribute the NE emission to the diffuse galactic O VI background. This enabled us to subtract the NE as a background from the NW data to further eliminate airglow lines, the diffuse UV emission and the galactic O VI background. The intensities of the airglow lines at 1042Å and 1048Å are quite similar in both the NE and NW, further allowing this subtraction. The raw spectra of the NW and the NE regions are shown in Figure 2, with airglow lines marked.

For the NW region, a nonlinear chi-squared minimization routine was used to fit Gaussian line profiles to the spectra. The wavelengths considered for analysis were restricted to 1010-1050 Å to minimize spurious background effects near the ends of the detector’s spectral range. The data were binned by 0.1 Å to increase the number of counts per bin without losing resolution, as the line widths were several Angstroms wide. The width of the broad H α line, from GWRL02, is $v_H = 2290 \text{ km s}^{-1}$. Since the Ly- β line is formed by the same process (Chevalier, Kirshner, & Raymond 1980), its line width was set equal to the H α broad component width. The shift of the centroid of the broad and narrow component of H α , $v = 29 \text{ km s}^{-1}$, is effectively negligible (implying that the shock is viewed completely edge-on) so the broad Ly- β line centroid was fixed at its rest wavelength. Only the intensity of the line was a free parameter. The blue wing of the line was fit from 1010 Å to 1024.5 Å. Due to the extinction from interstellar dust, a correction factor must be applied to deredden the observed flux. Using the extinction curves of Cardelli, Clayton, Mathis (1989), the resulting dereddened Ly- β flux is $2.3 \pm 0.3 \times 10^{-13}$ erg $\text{cm}^{-2} \text{s}^{-1}$.

After subtracting the fitted broad Ly- β line profile, the wavelength range from 1022-1028 Å was excluded from the fitting routine in order to avoid negative fluxes and residual airglow

that would skew the gaussian fits of the O VI lines. At ~ 1037.0 Å there were absorption features present that coincided with a C II line and molecular hydrogen lines, along with an O I airglow line. The absorption feature with the spectral range from 1035 - 1038 Å was therefore excluded from the fit.

The O VI doublet was fit with two gaussians with fixed centers at 1031.91 and 1037.61 Å respectively corresponding to the centroid of H α . The doublet line intensities were forced to have a 2:1 ratio but the magnitude of the intensities were allowed to vary. The observed flux is $6.7 \pm 0.1 \times 10^{-17}$ erg cm $^{-2}$ s $^{-1}$ arcsec $^{-2}$. Total dereddened flux for the O VI doublet lines was $1.8 \pm 0.2 \times 10^{-13}$ erg cm $^{-2}$ s $^{-1}$. The O VI line widths were measured to be 7.2 ± 0.4 Å FWHM, or equivalently 2100 ± 100 km s $^{-1}$. The formal error on the fit is 100 km s $^{-1}$. However, due to systematic error a more conservative error of ± 200 km s $^{-1}$ is used. The fits are shown in Figure 3. The width is within the limiting estimate of Raymond, Blair, Long (1995) of ≤ 3100 km s $^{-1}$ and is within 1σ error of the H α width of 2290 km s $^{-1}$. Although the faint signal in the NE did not allow for a statistically significant fit, an upper limit of O VI intensity was found assuming a width of 2000 km s $^{-1}$. The observed upper limit on the O VI line is 1.6×10^{-17} erg cm $^{-2}$ s $^{-1}$ arcsecond $^{-2}$. An upper limit on the dereddened intensity of O VI in the NE is 4.2×10^{-14} erg cm $^{-2}$ s $^{-1}$. The upper limit of flux for Ly- β in the NE is 1.6×10^{-17} erg cm $^{-2}$ s $^{-1}$ arcsecond $^{-2}$. An upper limit to the dereddened Ly- β intensity in the NE region is 4.4×10^{-14} erg cm $^{-2}$ s $^{-1}$.

Past observations of SN1006 line widths and intensities are summarized in Table 1. In order to compare past measurements made with varying aperture sizes, we use intensity per arcsecond measured along the length of the filament. The Ly- β from the HUT and the current FUSE observation are consistent. We can use the various measurements to study the ion heating. The proton temperature was found using the shock speed of 2890 km s $^{-1}$ from GWRL02. This proton temperature was then multiplied by m_{ion}/m_p to calculate the mass proportional temperatures. These calculated temperatures were then compared to the temperatures given by using the FWHM of each ion line. The temperature of O VI as indicated by its FWHM is less than mass proportional by 48%. For the other ions, He II, C IV the heating was also less than mass proportional, by 21% and 18% respectively.

The brightness of the O VI lines is proportional to density, n_0 , and the depth of the filament along the line of sight. Therefore, an upper limit to the density in the NE can be found by the ratio of intensities provided that the depths along the line of sight are known. Long et al. (2003) calculated a density ratio of $n(NW)/n(NE) = 2.5$. From the thermal component of the Chandra X-ray spectra Long et al. (2003) estimated a pre-shock ISM density of 0.25 cm $^{-3}$ in the NW. Using the limit to the O VI intensity ratio of the NW and NE a ratio of the densities is found to be $n(NW)/n(NE) \geq 4$, which is within the

uncertainties of the Long et al. calculations. Therefore, assuming a pre-shock density in the ISM of 0.25 cm^{-3} in the NW, the pre-shock NE density $\leq 0.06 \text{ cm}^{-3}$. This density calculation depends on the assumptions of similar depths along the line of sight in the NE and the NW and of similar numbers of O VI photons per atom passing through the shock. The amount of electron-ion equilibration in the NE would affect these assumptions. Greater electron-ion equilibration in the NE would increase the number of O VI photons per atom (Laming et al. 1996), so the limit on the density in the NE would be even smaller. We attribute the low upper limit on the O VI intensity in the NE to the low density medium into which the remnant is expanding.

4. Discussion

O VI lines were not conclusively observed in the faint non-radiative non-thermal NE shock indicating that the two distinct shock regions heat ions differently. Ion heating is important to cosmic ray acceleration and the overall energy distribution of the system. The ions have most of their kinetic energy in a broad distribution which is generally non-Maxwellian as the time to equilibrium via Coulomb collisions for ions and protons is 1.2×10^5 years. To understand the heating at the shock front, turbulence, line widths, methods of calculating heating, and the role of neutrals at the shock front will be discussed.

4.1. Small Scale Turbulence

Turbulence plays a role in the evolution of fast shocks in supernova remnants (Reynolds 2004; Ellison & Reynolds 1991). Small scale turbulence spreads the line profile of an ion much like thermal broadening of a line profile. Since some of the shock energy must be used for bulk flow, we will examine turbulence with a velocity of 1500 km s^{-1} which is large enough to affect the spectra but not contain all the energy of the flow. Turbulence decays on a time scale proportional to the characteristic length of the turbulence divided by the velocity of the turbulence $\sim \ell/v$ (Tennekes & Lumley 1972). The width of the H α filament is at most 10^{16} cm based on its $1''$ apparent width on the sky (GWRL02), making the time scale of the turbulence $10^8 \text{ s} \sim 3 \text{ years}$. Using this decay time and the post-shock speed of 750 km s^{-1} , one quarter of the shock speed, the post-shock region affected by turbulence would be $7.5 \times 10^{15} \text{ cm}$. The O VI filament with an observed width of $3 \times 10^{17} \text{ cm}$, assuming the $30''$ FUSE aperture is filled, is also too wide to be dominated by turbulence thus the turbulence that is present in the shock of SN1006 is short-lived and not a major source of line broadening.

4.2. Line Widths of O VI, UV lines and H α

The UV line profiles of the current observations can be compared with past observations of various ion species. The currently observed O VI line width in the NW shock is within 1σ of the H α line width previously measured by GWRL02. Vink et al. (2003) measured an O VII line width of 3.4 ± 0.5 eV, or approximately 1775 ± 261 km s $^{-1}$ from a different northwest region. This line width is substantially narrower than those of other ion species measured thus far, although the region of observation for this measurement is different from the position of our observations. Along a 124'' slit, Smith et al. (1991) found little variation in the H α profiles, indicating that the oxygen temperature does not vary significantly along the length of the NW filament. This implies one of two processes. First, the line width could decline with ionization state and distance behind the shock due to Coulomb collisions, as Coulomb collisions would transfer heat to other species. In Section 4.1, we found the Coulomb collision time to be far too long for this process to be important. The second more probable scenario is that some of the lower temperature O VII is from the reverse shock in the supernova ejecta. The detection of Si XIII and Mg XI X-ray lines (Long et al. 2003) in the NW region of the remnant agrees with the hypothesis that the emission is coming from ejecta near the shock front.

To find a proton temperature we have thus far used the width of the H α line. However, the proton thermal speed is not simply equal to the velocity derived from the width of the H α line at high temperatures. The cross section for neutral-proton charge transfer, the process that produces the broad H α , falls off at high energies allowing for the neutral hydrogen distribution function to be narrower than that of the protons (Chevalier, Kirshner, & Raymond 1980). This results in an H α profile that would incorrectly indicate a lower temperature than the actual proton temperature.

4.3. Heating at the Shock Front

From the current observations there are two ways to calculate the temperature of the ions. The first method to calculate the temperature is based on the thermalization of the bulk velocity of the shock. The second method uses the FWHM of the gaussian line fits as the thermal velocity that can be used to find the temperature. To determine the kinetic temperature of a species from the bulk thermalization we use the equation,

$$kT_i = \frac{3}{16}m_i v_{\text{shock}}^2 \quad (1)$$

where the subscript i indicates the species, k is the Boltzman constant, T is temperature, m_i

is the mass of the species and v_{shock} is the shock speed = 2890 km s^{-1} (GWRL02). This gives a temperature for O VI of $2.9 \times 10^9 \text{ K}$ and for the protons of $1.8 \times 10^8 \text{ K}$. The ratio of the temperatures is mass proportional, $T_{\text{oxygen}} = 16T_{\text{proton}}$, which is expected using this method. This heating occurs when some fraction of the energy of the shock speed is transferred to the thermal velocity of the protons or ions.

Using the width of the O VI lines to calculate temperature, the temperature is measured to be $1.5 \times 10^9 \text{ K}$. The O VI temperature derived from the observed line width is less than that predicted by the kinetic temperature equation for no equilibration among particle species. The ratio of the temperatures indicates that O VI is heated to a temperature 48% less than the value predicted for mass proportional heating. Ions are being heated by a process other than the bulk fluid velocity thermalization or there is a heat loss mechanism for the ions.

Heating of ions in collisionless shocks has been studied by Berdichevsky et al. (1997) using heliospheric shock data. In examining O VII, it was found that the oxygen was preferentially heated 19-39 times more than the protons. In studying the solar wind, Lee & Wu (2000) assume greater than mass-proportional heating as part of the coronal heating process. As a consequence, ions non-adiabatically expand upstream (not being reflected by the shock front) and move with a velocity equal to their gyration velocity as they go upstream. These hot highly energized ions could act as a precursor that takes away a significant amount of energy.

The current supernova observation of less than mass proportional heating lies in stark contrast to the heliospheric collisionless shocks. Several factors and processes determine the extent of ion heating. The first comparison to be made is the speed of the shock relative to the local Alfvénic speed. The solar shocks propagate at $400\text{-}1000 \text{ km s}^{-1}$. SN1006’s shock is propagating at almost 3000 km s^{-1} . The Alfvénic Mach number, the ratio of the shock speed to the square root average of the thermal and local Alfvénic speed, is ≤ 10 for solar shocks but upwards of 200 for the supernova shock. The orientation of the magnetic field with respect to the normal of the shock front is also of importance as quasi-perpendicular shocks and quasi-parallel shocks are quite different. If the current magnetic field orientation for SN1006 is correct, the NW is propagating parallel to the ambient magnetic field, while both parallel and perpendicular shocks are observed in the solar wind.

A measure of the importance of the magnetic field is the parameter β . The plasma β , the ratio of thermal to magnetic pressure upstream, is small (≤ 1) for heliospheric shocks. Using the parameters for SN1006 and the general value for the Galactic plane ISM magnetic field ($\sim 3 \mu\text{G}$), the NE has $\beta = 0.02$ and in the NW $\beta = 0.1$. This indicates that the magnetic field pressure dominates over the thermal pressure at the ISM/remnant boundary as in the

solar wind, in contrast to the ISM which is assumed to have a β of unity. It is possible that the change in density from pre-shock to post-shock conditions is an important characteristic in the propagation and heating of ions in the collisionless shock fronts.

In order to determine the cause of the different heating found in the heliosphere and the supernova further investigation of the influence of pressure, density, Mach number and velocity on ion heating by the shock is necessary.

4.4. Neutrals at the Shock Front

In the analysis scheme used here from Chevalier & Raymond (1978) and Chevalier, Kirshner, & Raymond (1980), neutrals play a vital role. Neutrals undergo charge exchange or emit line radiation to produce the $H\alpha$ and Ly- β emission. There are fast neutrals produced by the shock, as evident by the broad components of the $H\alpha$ and Ly- β lines. This could create a neutral precursor for the shock (Smith et al. 1994; Lim & Raga 1996). The hydrogen and oxygen neutral fractions are tightly coupled by charge transfer, thus information about the neutral fraction of hydrogen can be used to diagnose the neutral fraction of oxygen. These neutrals should become pickup ions like those seen in the solar wind (Vasyliunas & Siscoe 1976) when they pass through the shock and become ionized. Pickup ions like those in the heliosphere can then act as a high energy seed population for Fermi acceleration just as heliospheric pickup ions are the seed population for anomalous cosmic rays (Fisk, Kozlovsky & Ramaty 1974).

The He II 4686Å line can be used as an indicator of neutral fraction due to its insensitivity to pre-shock neutral fraction and electron-ion pre-shock temperature equilibrium (GWRL02). In the NW, observations have shown He II emission lines (Raymond, Blair, Long 1995)(GWRL02). The ratio of He I/He II can then be used to find an H neutral fraction which is a parameter in the relation of the $H\alpha$ two component intensity ratio, $I_{\text{broad}}/I_{\text{narrow}}$, and the electron-ion temperature ratio. In addition, GWRL02 calculated the pre-shock H population to be 90% ionized but the pre-shock He population is 70% neutral. Using the $H\alpha$ broad-to-narrow intensity ratio calculated for 90% pre-ionized medium, the temperature ratio, $T_{\text{electron}}/T_{\text{proton}}$, was found to be ≤ 0.07 , showing little to no equilibration between protons and electrons. Using the ratio of $T_{\text{electron}}/T_{\text{proton}}$, we find an electron temperature of $\leq 1.2 \times 10^7$ K, approximately 1 keV, which is an upper limit that agrees with the value found by Long et al. (2003) of $T_{\text{electron}} \leq 0.6$ keV, but significantly less than the oxygen and proton temperatures found for this observation (1.5×10^9 K and 1.8×10^8 K, respectively).

5. Summary

In summary, the two shock regions of SN1006 studied here provide a unique cosmic laboratory for shocks and their acceleration processes. Clearly, the properties of the interstellar medium play a crucial role in shaping these shocks. We conclude with the following summary of our observations and interpretations.

1. The material that the NE shock front is encountering is less dense than in the NW region, with a ratio $n(\text{NW})/n(\text{NE}) \geq 4$, and is best seen in the X-ray or radio wavelengths. The NW shock front could be moving into a diffuse H I cloud or similarly dense region.
2. The O VI line width of the NW shock indicates that oxygen ions are heated to a temperature less than 48% of the value predicted by mass proportional heating. This differs from the observations of other non-radiative collisionless shock fronts such as those in the heliosphere which found ion temperatures 20-40 times in excess of the values predicted by mass proportional heating. The roles of density, pressure, magnetic field orientation with respect to the shock normal, velocity and Mach number should be examined to better determine the ion heating mechanisms.
3. The plasma at the shock front has not had time to come to equilibrium via Coulomb collisions. The plasma is in a non-equilibrium state with energy distributed differently between species of the plasma. This is in agreement with the work on temperature equilibrium done by Ghavamian et al. (2002) who found the ratio of proton to electron temperature to be ≤ 0.07 indicating a plasma far from equilibrium.

The role of the neutral fraction of the ISM population in the charge exchange interaction should be examined in detail as it may greatly affect the outcome of the shock-ISM interaction. The rate at which the plasma becomes isotropic, the particle distribution, and the time scale to reach isotropic and Maxwellian conditions are in need of examination to understand the heating process present in the collisionless shock. Further work will be done to model the plasma conditions in collisionless shock fronts to include neutral fraction as well as examine the role of electron population on O VI formation. This work should help advance the understanding of the shock acceleration of particles and the physics of a collisionless shocks in varying environments.

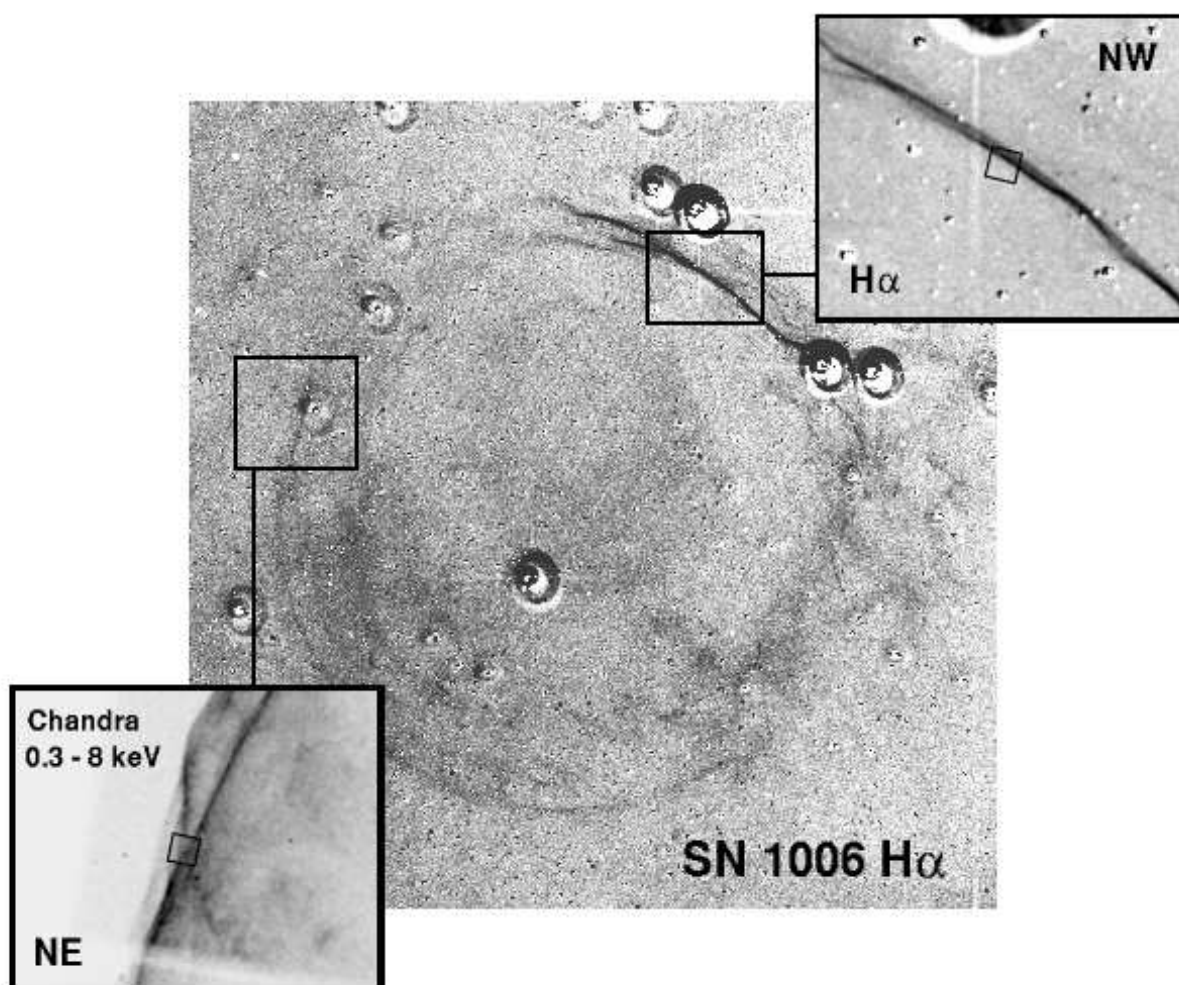
This work is based on observations made with the NASA-CNES-CSA Far Ultraviolet Spectroscopic Explorer. FUSE is operated for NASA by the Johns Hopkins University

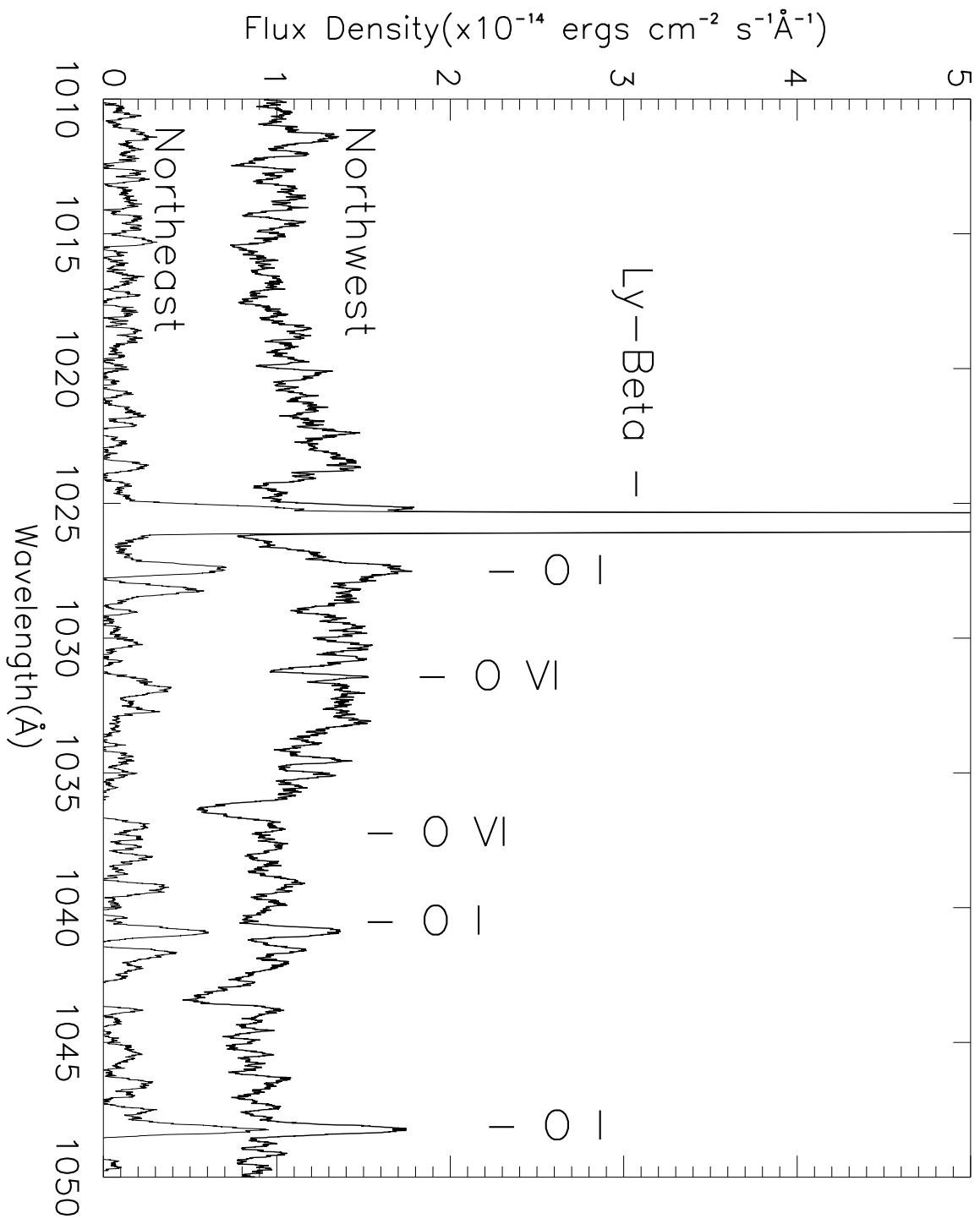
under NASA contract NAS5-32985. We gratefully acknowledge conversations and help with FUSE night only data extractions by R. Sankrit. This work is supported by NASA Grant number NEG5-10352 given to the Smithsonian Observatory. K. Korreck is supported by the University of Michigan NSF-Rackham Engineering Award. This work made use of the NASA Astrophysics Data System (ADS).

REFERENCES

- Anderson, B. G., Sankrit, R., Dupuis, J., 2003, FUSE Observer’s Guide
- Bamba, A., Yamazaki, R., Ueno, M., Koyama, K., 2003, ApJ, 589, 827
- Berdichevsky, D., Geiss, J., Gloeckler, G., Mall, U., 1997, J. Geophys. Res., 102, 263
- Cardelli, J. A., Clayton, G. C., Mathis, J. S., 1989, ApJ, 345, 245
- Chevalier, R. A., Kirshner, R. P., Raymond, J. C., 1980, ApJ, 235, 186
- Chevalier, R. A., Raymond, J. C., 1978, ApJ, 225, L27
- Dyer, K. K., Reynolds, S. P., Borkowski, K. J., 2004, ApJ, 600, 752
- Ellison, D.C., Reynolds, S. P., 1991, ApJ, 382, 242
- Fisk, L. A., Kozlovsky, B., Ramaty, R. 1974, Astrophys. Lett., 190, L35
- Ghavamian, P., Winkler, P. F., Raymond, J. C., Long, K. S. 2002, ApJ, 572, 999
- Hester, J. J., Raymond, J. C., Blair, W. P., 1994, ApJ, 420, 721
- Henry, R. C., Murthy, J., 1993, ApJ, 418, L17
- Jones, L. R., Pye, J. P., 1989, MNRAS, 238, 567
- Kirshner, R. P., Winkler, P. F., Chevalier, R.A., 1987, ApJ, 315, L135
- Laming, J. M., Raymond, J. C., McLaughlin, B. M., Blair, W. P., 1996, ApJ, 472, 267
- Lee, L. C., Wu, B. H., 2000, ApJ, 535, 1014
- Lim, A. J., Raga, A. C., 1996, MNRAS, 280, 103
- Long, K. S., Reynolds, S. P., Raymond, J. C., et.al. 2003, ApJ, 586, 1162

- Mancuso, S., Raymond, J. C., Kohl, J., et. al. 2002, *A&A*, 383, 267
- Murthy, J., 2002, *AJ*, 23, 23
- Murthy, J., Henry, R. C., 1995, *ApJ*, 448, 848
- Otte, B., Dixon, W. V., Sankrit, R., 2003, *ApJ*, 586, L53
- Otte, B., Dixon, W. V., Sankrit, R., 2004, *ApJ*, preprint
- Pye, J. P., Pounds, K. A., Rolf, D. P., Smith, A., Willingate, R., Seward, F. D., 1981, *MNRAS*, 194, 569
- Raymond, J. C., Blair, W. P., Long, K. S., 1995, *ApJ*, 454, L31
- Reynolds, S. P., 2004, *Adv. Space Res.*, 33, 461
- Reynolds, S. P., 1996, *ApJ*, 459, L13
- Reynolds, S. P., Chevalier, R. A., 1981, *ApJ*, 245, 912
- Reynolds, S. P., Gilmore, D. M., 1986, *AJ*, 92, 1138
- Schweizer, F., Middleditch, J., 1980, *ApJ*, 241, 1039
- Shelton, R. L., 2002, *ApJ*, 569, 758
- Shelton, R. L., Kruk, J. W., Murphy, E. M., et al., 2001, *ApJ*, 560, 730
- Smith, R. C., Kirshner, R. P., Blair, W. P., Winkler, P. F., 1991, *ApJ*, 375, 652
- Smith, R. C., Raymond, J. C., Laming, J. M., 1994, *ApJ*, 420, 286
- Spitzer Jr., L., 1956, 'Physics of Fully Ionized Gases', Interscience Publishers, Inc.
- Tennekes, H., Lumley, J.L., 1972, 'A First Course in Turbulence', The MIT Press
- Tanimori, T., 1998, *IAU Circ.*, 188, 121
- Vasyliunas, V. M., Siscoe, G. L., 1976, *J. Geophys. Res.*, 81, 1247
- Vink, J., Laming, J. M., Gu, M. F., Rasmussen, A., Kaastra, J. S., 2003, *ApJ*, 587, L31
- Willingdale, R., West, R. G., Pye, J. P., Stewart, G. C., 1996, *MNRAS*, 278, 749
- Winkler, P. F., Gupta, G., Long, K. S., 2003, *ApJ*, 585, 324





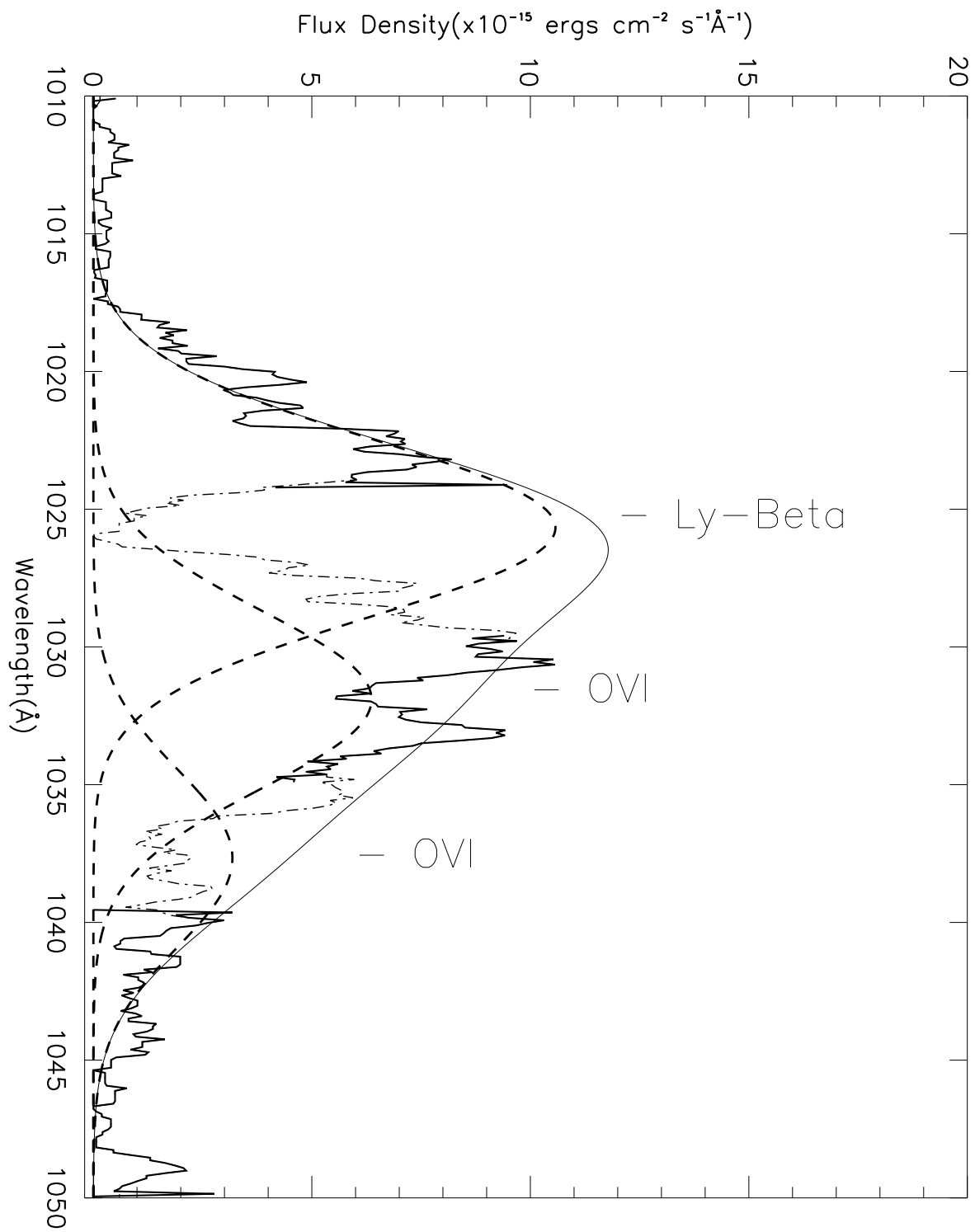


Fig. 1.— $H\alpha$ image of SN1006 taken by the CTIO Schmidt telescope from Winkler et al. (2003). Closeup images of the observed filaments are shown in the insets. In each case the interior box, drawn to scale, shows the location of the $30'' \times 30''$ FUSE LWRS aperture. The NW blowup is from the same $H\alpha$ image while the NE blowup is a 0.3-8 keV Chandra image (Long et al. 2003).

Fig. 2.— Raw FUSE spectra from the Northeast and Northwest region of SN1006. The NW is offset from the NE by 0.5 for clarity. Geocoronal lines are marked. The $Ly-\beta$ peak dominates in both spectra. The NE is consistently fainter than the NW, but the geocoronal line intensities are similar.

Fig. 3.— FUSE spectra from the NW, binned at 0.1 \AA with the NE subtracted as background. The dotted dashed lines are the regions of the spectra that were excluded from the fits. The dashed lines are the fits for the $Ly-\beta$, O VI 1032 and 1037 \AA lines, with FWHM of 2290 and 2100 km s^{-1} respectively. The solid line represents the addition of the fits of the three spectral lines.

Table 1. Summary of UV Emission Lines in NW Filament of SN1006

Ion	Intensity (photons $\text{cm}^{-2}\text{s}^{-1}\text{arcsec}^{-1}$) ($\times 10^{-4}$)	Filament Length (arcsec)	FWHM (km s^{-1}) Observed	Temperature (Kelvin) from FWHM	$m_{ion}/m_p T$ (Kelvin)	% Mass Prop
H- α ¹	2.1	51	2290 ± 80	1.8×10^8 ^a	-	-
Ly- β	4.0	30	2290(fixed)	-	-	-
He II ²	0.99	197	2558 ± 618	5.7×10^8	7.2×10^8	79%
C IV ²	1.7	197	2641 ± 355	1.8×10^9	2.2×10^9	82%
O VI	3.1	30	2100 ± 200	1.5×10^9	2.9×10^9	52%
O VII ³		60	1775 ± 261	1.1×10^9	2.9×10^9	38%

^aTemperature derived from shock speed of 2890 km s^{-1} .

References. — (1) Ghavamian et al. 2002; (2) Raymond et al. 1995; (3) Vink et al. 2003